13th International Symposium on Turbulence and Shear Flow Phenomena (TSFP13)
Montreal, Canada, June 25–28, 2024

BOUNDARY LAYER DEVELOPMENT UNDER STREAMWISE PRESSURE GRADIENTS AT HIGH REYNOLDS NUMBERS OVER ROUGH WALLS

Thomas Preskett
Department of Aeronautics and Astronautics
University of Southampton
University Rd, Southampton SO17 1BJ
tdp1g17@soton.ac.uk

Bharathram Ganapathisubramani
Department of Aeronautics and Astronautics
University of Southampton
University Rd, Southampton SO17 1BJ
g.bharath@soton.ac.uk

ABSTRACT

Building on the limited previous studies on the effect of non-equilibrium pressure gradients on the structures of a turbulent boundary layer over a rough wall. Experiments were conducted at the University of Southampton in the 12m boundary layer wind tunnel. Particle image velocimetry (PIV) was used to capture the flow over a rough wall under the influence of pressure gradients. The pressure gradient is applied using a NACA0012 aerofoil of 1.25m chord with measurements taken from one chord upstream to one chord downstream. A two-point spatial correlation coefficient is used to analyse the coherence of the motions in the flow. When looking at $R_{u'u'}$, it is seen that a favourable pressure gradient results in longer contours, while an adverse pressure gradient is shorter. For contours $R_{u'u'} = 0.2$, the correlation length reduces as the reference point moves away from the way. While for $R_{u'u'} = 0.6$, the correlation length remains relatively constant as y_{ref} increases.

INTRODUCTION

Pressure gradient effects have been extensively studied on smooth walls, with more limited studies on rough walls. Many of these studies focus on the effect of the pressure gradient on the mean velocity profiles. Adverse pressure gradients have been seen to increase the wake strength while reducing the length of the log region (Monty *et al.* (2011)). While works such as Tay *et al.* (2009) show that favourable pressure gradients cause smaller wake strengths and thinner boundary layers. It is also well known that favourable pressure gradients increase local skin friction while adverse pressure gradients reduce skin friction (Monty *et al.* (2011) and Shin & Song (2015)).

Two-point correlation can be used to identify the coherent structures within a flow. Previous work, including Sillero *et al.* (2014), shows spatial correlation contours for smooth wall ZPG boundary layers. They showed coherent structures of 7δ for the weakest correlated structures. This work aims to build on past work and present spatial correlation at a given point with different pressure gradient histories. The key question to be answered is the effect of different pressure gradients on the streamwise correlation length. Furthermore, how does the reference location height affect the size of these coherent motions?

METHODOLOGY

Experiments are carried out in the University of Southampton's 12m boundary layer with a tunnel with a cross-section of 1.2x1m. A NACA0012 aerofoil of chord 1.25m is mounted from the tunnel roof to allow different pressure gradient histories to be imposed upon the flow. The leading edge is located 6.5m downstream of the inlet of the wind tunnel. The quarter chord was kept 500mm above the tunnel floor, upon which the 3mm thick chicken wire mesh is mounted. Five different pressure gradient histories are captured using particle image velocimetry (PIV) at angles of attack from -8° to 8° in steps of 4°. PIV was taken from one chord upstream of the leading edge to one chord downstream of the trailing edge. This was achieved using three Lavision ImagerProLX 16MP cameras in four different positions with the laser sheet pointing upstream to prevent the optics from affecting the flow. This sheet was created using a Litron Bernoulli 200-15 Nd:YAG laser with a beam of 523nm wavelength using Lavision sheet optics. A diagram of this setup can be seen in figure 1 for the most downstream measurements, with the blue boxes showing the three fields of the view of the cameras. The cameras and laser were moved four times to cover the flow domain. Three cameras give approximately 1m field of view to consider the correlation. At the same time, the mean fields are available for all three chords of interest. For each case, 2000 images were captured to ensure good statistical convergence. Throughout the experiment, the data was taken at 20m/s, set by the pitot, one chord upstream of the aerofoil. The pressure gradient history is measured using 16 taps along the tunnel floor, shown in figure 1 by the small vertical lines. These are scanned using a ZOC 33/64 pressure scanner to measure the mean pressure distribution. The colours and line styles used for plotting are given in table 1.

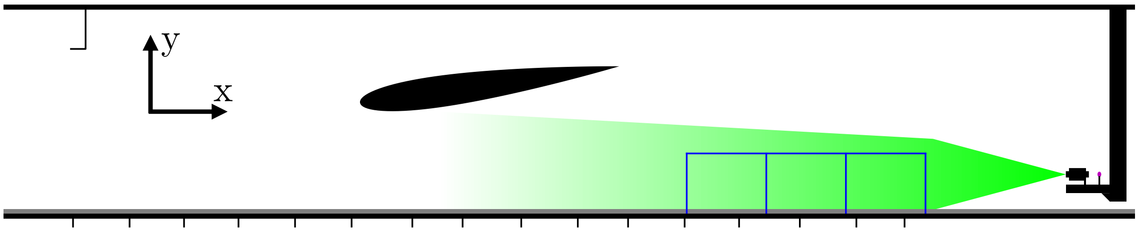

Figure 1. Diagram showing the experimental setup for the first position with blue boxes showing the field of view of the three cameras. The pitot tube is located at 5.3m from the inlet of the wind tunnel and is one chord upstream of the aerofoil leading edge.

	$-8°$	$-4°$	$0°$	$4°$	$8°$
Symbol	●	▼	■	◆	▲
Line	solid	dashed	dotted	dash-dot	dash-dot-dot

Table 1. The colours used for each angle of attack throughout this paper. The makers are used for data points, while lines of the same colours will be used for PIV data

RESULTS

This section will look at some results of the experiment, first looking at the pressure gradient histories and then at the correlation within the flow.

Pressure Gradient Histories

These experiments look at the effect of different pressure gradient histories, and thus, first, we look at the imposed pressure gradient. The angle of attack is varied to give varying pressure gradient histories, presented in figure 2. As required for the experiments, it can be seen there is good variation between the different pressure gradient cases. The $-8°$, $-4°$ and $0°$ cases have a favourable pressure gradient followed by an adverse pressure gradient. Meanwhile, the $4°$ and $8°$ have an adverse pressure gradient followed by a favourable one. Significantly, for these experiments, the magnitude of the pressure gradient varies in strength and order. Furthermore, there is a crossover point at the quarter chord where all the pressure gradients are equal, around -0.25. The position of the taps relative to roughness elements causes the pressure gradient history to look bumpy.

The pressure gradient history can also be shown using the acceleration parameter K given by $K = (\nu/U_1^2)dU_1/dx$ where U_1 is the local freestream velocity. To calculate K, the local freestream velocity is required; for these experiments, we have two methods to find this. The first is from the PIV data. We can take the boundary layer edge velocity and estimate the velocity from the pressure data. The results of these two methods are shown in figure 3. The results show good agreement between the pressure and PIV data in determining the freestream velocity. This is a useful result since taking PIV data over the whole domain of interest is often impractical, but parameters such as K may be required to predict the flow. Therefore, using pressure taps or other methods, which are much simpler to take measurements, enables estimates of the flow history to be calculated.

The distribution of K is shown in figure 4 for the five angles of attack. In favourable pressure gradient regions, K is positive, while in adverse pressure gradient regions, K is negative. This is expected from Bernoulli's equation since the velocity gradient equals $-(1/\rho)(dP/dx)$. We can study flow his-

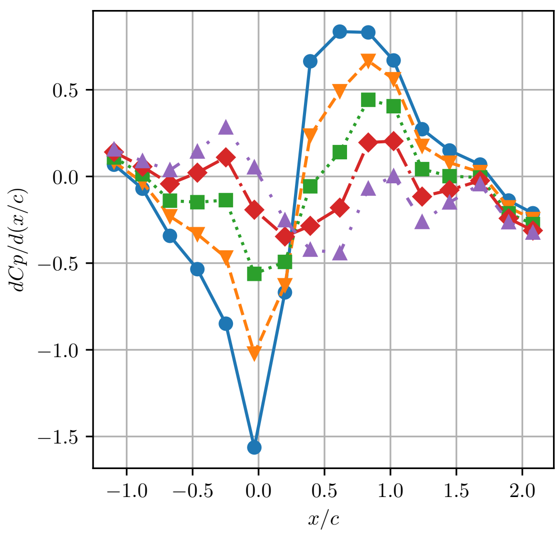

Figure 2. Pressure gradient with respect to the normalised position x/c for the five angles of attack used in the experiment.

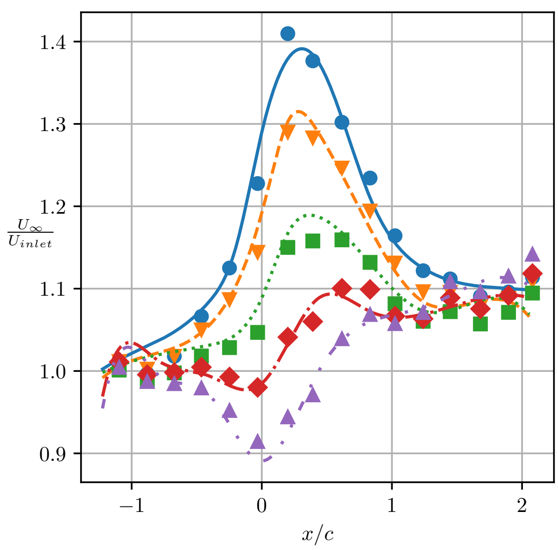

Figure 3. The freestream velocity variation from one chord upstream to one chord downstream of the aerofoil. The markers show the edge velocity as predicted from the pressure distribution, while the dashed lines show the edge velocity from PIV.

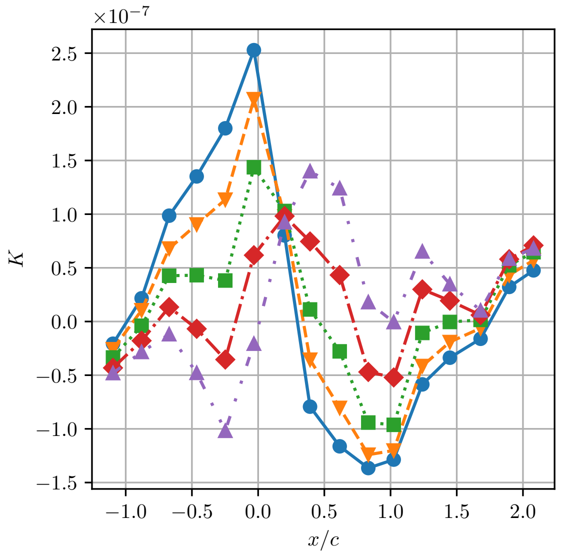

Figure 4. Acceleration parameter K for 20m/s cases from one chord upstream to one chord downstream of the aerofoil. Found using the local velocity from the pressure distribution at 20m/s.

tory using both K and the non-dimensional pressure gradient. However, a key difference between them is the $dCp/d(x/c)$ is invariant to the Reynolds number, but K is not, and the magnitude of the peak values reduces with speed.

Two Point Correlation

Two-point spatial correlation is carried out using equation 1 ((Pope, 2000, p.57)) on the fluctuations of the velocity fields captured. For the following results, the point of reference is kept constant at 6.85m from the inlet and at a height of 0.2δ to see how events at this point are correlated to those around it. This point corresponds to the quarter chord of the aerofoil where all cases have a pressure gradient of $dCp/d(x/c) \approx -0.33$. This point is interesting since all the cases have the same local pressure gradient; however, the upstream pressure gradient histories differ.

$$R_{u'u'} = \frac{< u'_1 u'_2 >}{\sqrt{< u'^2_1 >< u'^2_2 >}} \tag{1}$$

Starting with the $R_{u'u'}$, the field of view extends from x/c = -0.42 to 0.59, as shown in figure 5 for -8°. As expected, the correlation contour increases in length as the contour level is reduced. It is seen that a contour level of 0.2 extends approximately two δ upstream and downstream. While for a contour level of 0.8, the contour only extends from -0.1 to 0.1 of δ upstream and downstream. The contours of $R_{u'u'}$ have an elongated shape with a slight upward inclination.

Figure 6 looks at $R_{v'v'}$ for -8° and the areas within the correlation contours are much smaller. It is also seen while $R_{u'u'}$ gives contours that are elongated, the $R_{v'v'}$ contours are much more circular. This means that the fluctuations of v influence each other much less than those of the U component. While for $R_{u'u'}$, there is a region of limited correlation that extends from -4δ to the edge of the field of view. This region is much smaller for $R_{v'v'}$, with correlation only seen from approximately -1δ to 1δ.

	-8°	-4°	0°	4°	8°
$\frac{1}{1.25}\int_{-1}^{0.25} \omega \frac{dCp}{d(x/c)}$	-0.22	-0.14	-0.05	0.03	0.09

Table 2. Values of $\frac{1}{1.25}\int_{-1}^{0.25} \omega \frac{dCp}{d(x/c)}$ from one chord upstream to the quarter chord of the aerofoil. ω is a linear weight from 0 one chord upstream to 1 at the quarter chord.

The final whole flow field to look at is $R_{u'v'}$, where U component fluctuations at the reference point correlate with V component fluctuations. When a component is correlated with itself, the value is expected to lie between -1 and 1. However, when the two components are correlated, the min value is -0.46, and the max is 0.3 across all angles. The field of $R_{u'v'}$ for -8° is shown in figure 7. While for $R_{u'u'}$ and $R_{v'u'}$, the correlation near the reference value is positive for $R_{u'v'}$, it is negative. On average, positive u' values are associated with negative v' and vice versa. This, as expected, means momentum is transported towards the wall on average.

The next observation that can be made is that the correlation area extends upstream more than downstream. This differs from the cases above, which extend further downstream than upstream. This means that reference location is more influenced by upstream events than it influences downstream events.

Effect Of Pressure Gradient History On Correlation Shape

The above work looked at the correlation for different contour levels for a single angle of attack. This section looks at a single contour level and how that shape is affected by different pressure gradient histories.

Figure 8 shows the contour for a correlation coefficient value of $R_{u'u'} = 0.4$ for the five angles of attacks tested. It is seen that there are two groups for the shape of contours, one that contains -8°, -4° and 0° and one that contains 4° and 8°. As seen in figure 2, the first group experiences a predominately favourable pressure gradient. Meanwhile, the second group predominately experienced an adverse pressure gradient. One way to quantify this pressure gradient is to take linear weightings from 0 one chord upstream to 1 at the quarter chord and determine an integral value of the pressure gradient. These results are shown in table 2. It shows that the first group do indeed have a favourable pressure gradient, and the other has a net adverse pressure gradient.

For the contour level of 0.4, it can be seen that even though the 4° and 8° cases, the shape and size of the contour are nearly identical. This is despite having different pressure gradient histories as seen in table 2. The other three cases show a little more variation but are still similar. Despite the -4° case having a more favourable integral pressure gradient, its shape is similar to the 0° case. The strongest favourable pressure gradient of the -8° cases shows the contour starting higher above the wall. One reason for this may be due to the thinner boundary layer. Due to near-wall reflections, etc, these extend into a greater proportion of the boundary layer. The results suggest that the favourable pressure gradient extends the correlation of u' with u' further downstream than the adverse pressure gradient. This difference is due to the higher flow speeds and, thus, momentum within the flow for the favourable pressure gradient cases. This is seen in figure 3 where the freestream velocity increases for -8°, -4° and 0° while decreasing for the other two. This suggests that the favourable pressure gradient elongates the structures within the flow. The correlation

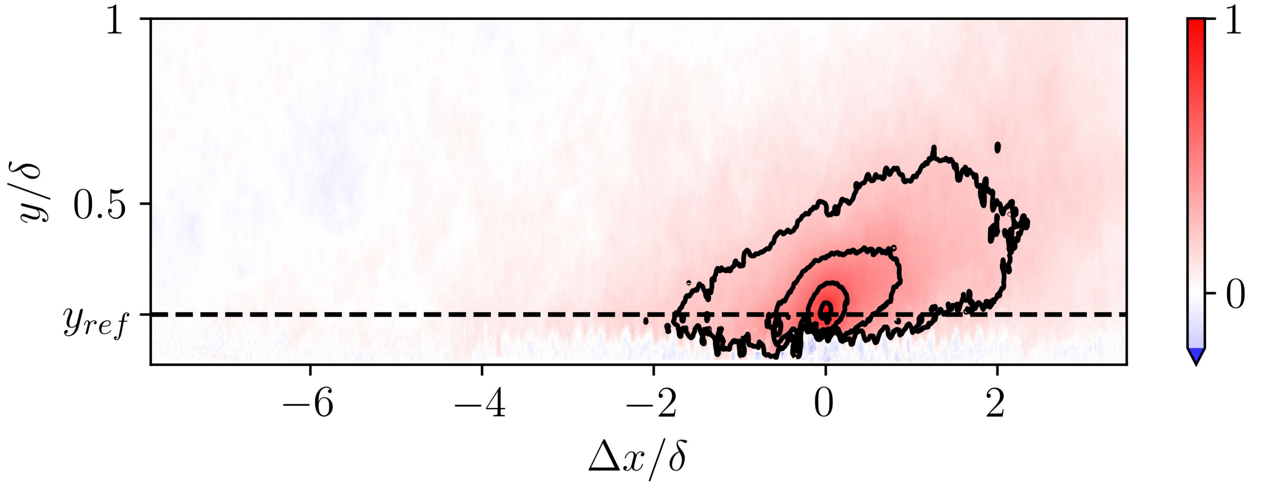

Figure 5. Field of $R_{u'u'}$ referenced to (6.85m, 0.2δ) for $-8°$ case. Contours of correlation levels corresponding to 0.2, 0.4, 0.6 and 0.8 are shown. y_{ref} is taken to be 0.2δ

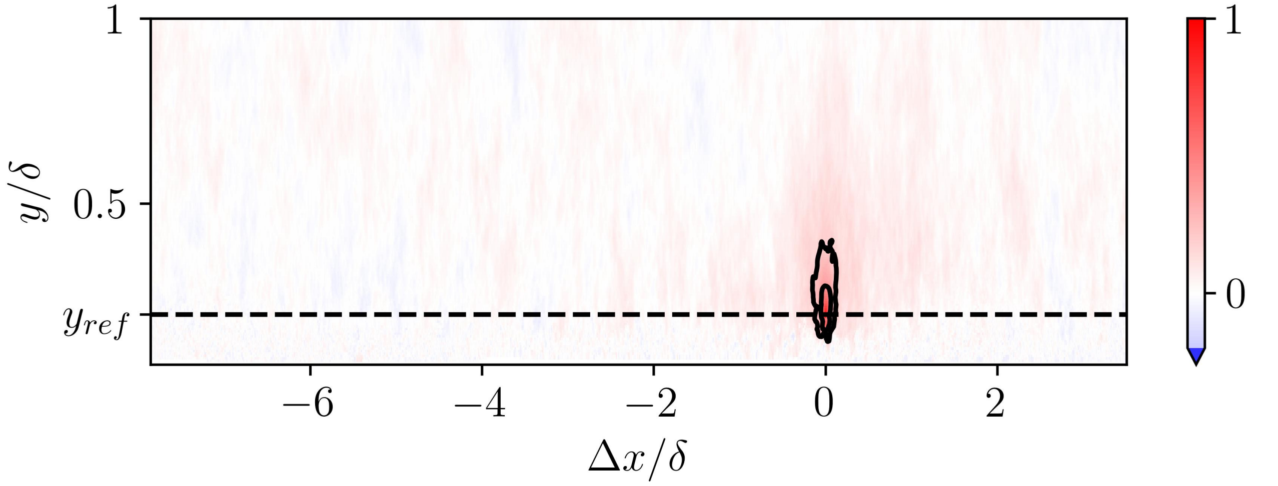

Figure 6. Field of $R_{v'v'}$ referenced to (6.85m, 0.2δ) for $-8°$ case. Contours of correlation levels corresponding to 0.2 and 0.4 are shown. y_{ref} is taken to be 0.2δ

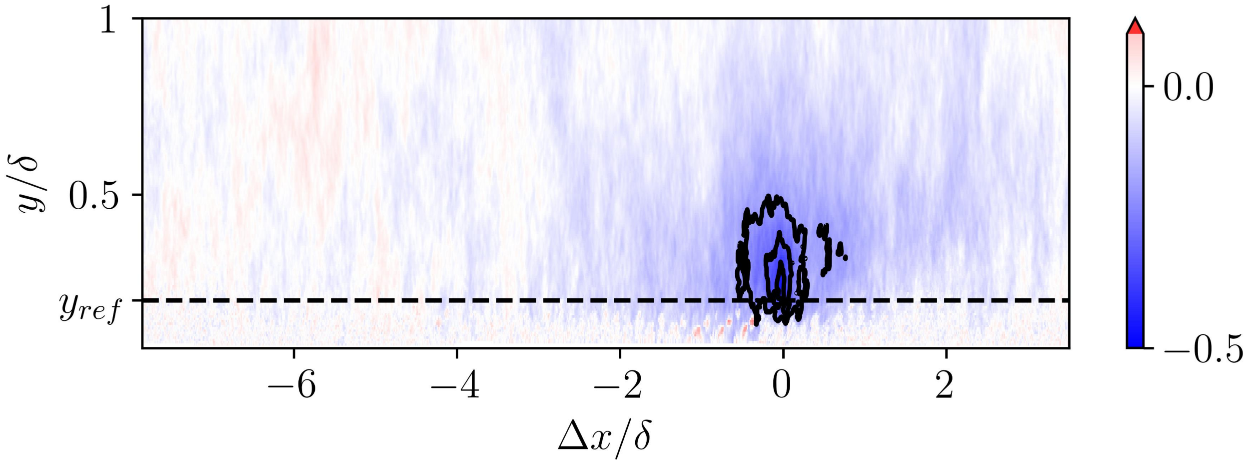

Figure 7. Field of $R_{u'v'}$ referenced to u' at (6.85m, 0.2δ) for $-8°$ case. Contours of correlation levels corresponding to -0.2, -0.3 and -0.4 are shown. y_{ref} is taken to be 0.2δ

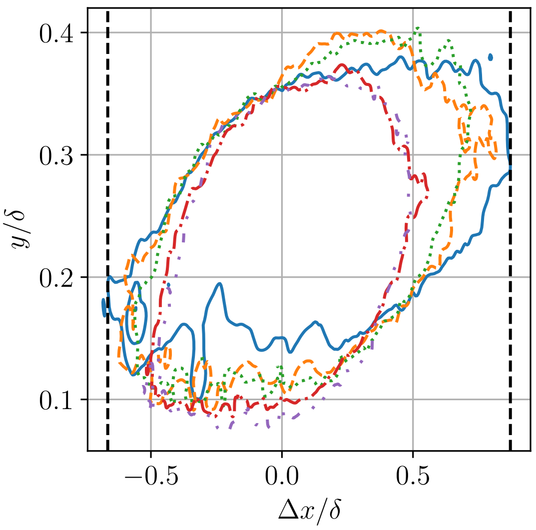

Figure 8. Contours of $R_{u'u'}$ for correlation level of 0.4 for different angles of attack. The black vertical dashed lines show now the streamwise correlation length is to be defined for the $-8°$ case. The reference position is 6.85m (x/c = 0.25) and 0.2δ. Line styles are given in table 1.

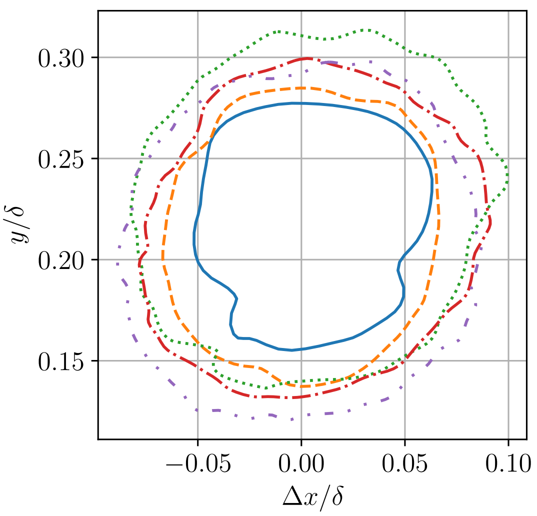

Figure 9. Contours of $R_{v'v'}$ for correlation level of 0.4 for different angles of attack. The reference position is 6.85m (x/c = 0.25) and 0.2δ. Line styles are given in table 1.

area also extends higher into the boundary layer than with an adverse pressure gradient.

Having looked at the correlation of the U component, we move on to look at the V component in figure 9 again at contours of $R_{v'v'}$ = 0.4. There is no clear grouping of the cases seen for $R_{u'u'}$ contours. There is some order to the results; the strongest favourable pressure gradient of the $-8°$ case results in the smallest contour area. However, all the cases have similar areas of influence, with no clear trend seen in the results. As was seen for contours of $R_{u'u'}$, the shape of the adverse pressure gradient cases are very similar, and this is because the upstream pressure gradients result in very similar integral pressure gradient values. As was seen in figure 6, the contours are much more circular than those of $R_{u'u'}$.

The final correlation is $R_{u'v'} = -0.3$, and there is a similar

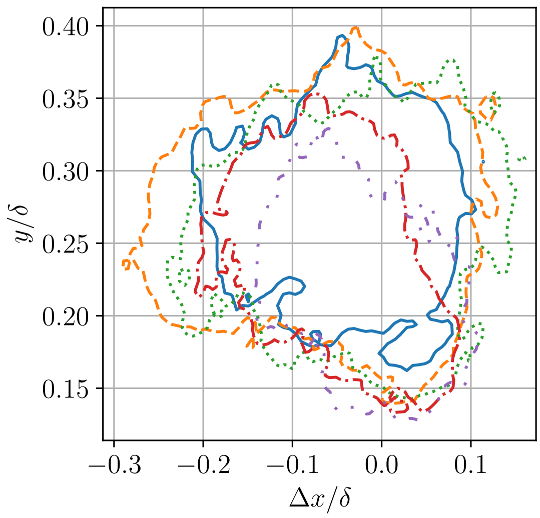

Figure 10. Contours of $R_{u'v'}$ for correlation level of -0.3 for different angles of attack. The reference position is 6.85m (x/c = 0.25) and 0.2δ. Line styles are given in table 1.

grouping as seen in figure 8. It is seen that a favourable integral pressure gradient increases the downstream correlation area compared to the adverse pressure gradient cases. The adverse pressure gradient cases show a smaller area for the given level than the favourable pressure gradient cases. The trend is seen in figure 7 where the contours extend further upstream than they do downstream.

Effect Of Pressure Gradient History On Streamwise Correlation Length

The above work looks at one y_{ref} location at $y/\delta = 0.2$ and how the shape of the contours changes for different values of $R_{u'u'}$. The contour levels can be seen to represent the size of the structures within the flow. A contour level closer to 0 can represent the larger structures within the flow, while a higher contour level closer to 1 represents smaller structures. Defining a length scale to examine the structures within the flow is possible. For this analysis, we will use the streamwise correlation length. In figure 8, two black dashed lines show the min and max on the contour for $-8°$ case. The streamwise correlation length is defined as the distance between these two lines. Since some levels will produce more than one contour for a given level, the maximum streamwise correlation length is taken for each location and angle of attack.

Figure 11 shows the variation in streamwise correlation length as the reference location height varies. The contour value is kept constant at 0.2 to start with, representing large-scale structures within the flow. It can be seen that there is an order to the cases valid for all y/δ locations. The $-8°$ case has the strongest favourable pressure gradient and has the largest streamwise correlation length. The 8° case, which experiences the adverse pressure gradient, is seen to have the shortest correlation length and thus structures within the flow. The other cases follow the order of the integral pressure gradients seen in table 2.

All the cases show a decreasing trend in the correlation length as the reference location height increases. In some cases, such as the $-8°$ case, there is an initial increase in the values; however, the overall trend is decreasing. This suggests that the structures reduce in length towards the boundary layer edge. The maximum variation between the max correlation

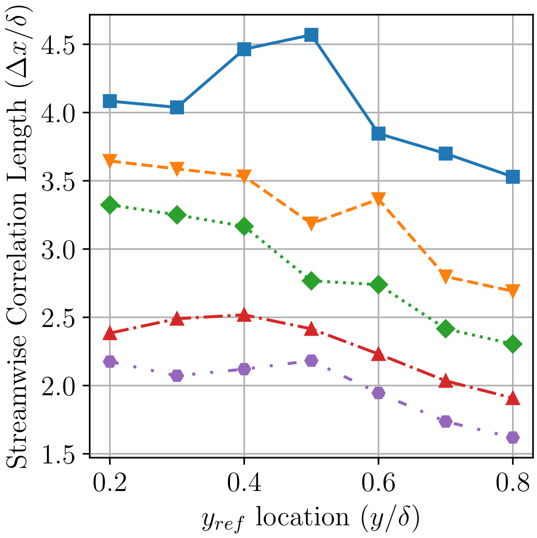

Figure 11. Streamwise correlation length for different angles of attack and different y/δ positions for a contour level of 0.2. The reference position is taken to 6.85m (x/c = 0.25). Line styles and symbols are given in table 1.

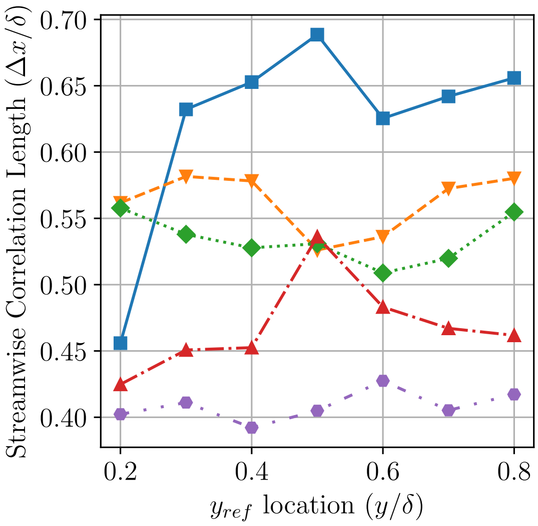

Figure 12. Streamwise correlation length for different angles of attack and different y/δ positions for a contour level of 0.6. The reference position is taken to 6.85m (x/c = 0.25). Line styles and symbols are given in table 1.

length and min correlation length is 44% for the 0° case, with the other cases showing around 30% difference.

Finally, we continue the above analysis for a different contour level of $R_{u'u'} = 0.6$ in figure 12. Overall, the trends are similar to those seen in figure 11. The favourable pressure gradient cases have the longest correlation length, and the adverse cases have the smallest. More scatter is seen in the results at a higher correlation level, and the streamwise correlation length, as seen above, reduces. The streamwise correlation length at this contour level appears invariant to the y_{ref} location. The exception is the $-8°$ case at a $y_{ref} = 0.2\delta$, which is much smaller than the other wall's normal positions. This seems an anomaly since all other cases follow the trend for the lower contour level of 0.2.

CONCLUSIONS

It has been seen that the pressure gradient histories have a clear effect on the structures within the flow. This has been investigated using two-point correlation and then looking at the resulting contours within the flow field. Plotting fields of $R_{u'u'}$ and $R_{v'v'}$ showed the contours of $R_{u'u'}$ results in large elliptical type contours elongated in flow direction with a upward inclination. While $R_{v'v'}$ results in tall thin contours smaller in height than for those seen in $R_{u'u'}$. Analysis of $R_{u'v'}$ shows the contours extended further upstream than they did downstream. The streamwise correlation length depends on the integral pressure gradient history. Cases with favourable pressure gradient showed a longer streamwise correlation length, while adverse pressure gradient cases were shorter. The order of cases was constant across all contour values of $R_{u'u'}$. However, for a contour value of 0.2, there was a reduction in the streamwise correlation length as the ref location was moved further away from the wall. For a higher correlation value of 0.6, representing the smaller structures within the flow, the correlation length was approximately invariant to the wall-normal position of the reference location. The correlation length was again seen to follow the order of the integral pressure gradient histories.

REFERENCES

Monty, J.P., Harun, Z. & Marusic, I. 2011 A parametric study of adverse pressure gradient turbulent boundary layers. *International Journal of Heat and Fluid Flow* **32** (3), 575–585.

Pope, S.B. 2000 *Turbulent Flows*. Cambridge: Cambridge University Press.

Shin, J.H. & Song, S.J. 2015 Pressure gradient effects on smooth and rough surface turbulent boundary layers-part i: Favorable pressure gradient. *Journal of Fluids Engineering, Transactions of the ASME* **137** (1).

Sillero, J.A., Jiménez, J. & Moser, R.D. 2014 Two-point statistics for turbulent boundary layers and channels at reynolds numbers up to $\delta^+ \approx 2000$. *Physics of Fluids* **26** (10).

Tay, G., Kuhn, D. & Tachie, M. 2009 Particle image velocimetry study of rough-wall turbulent flows in favorable pressure gradient. *Journal of fluids engineering* **131** (6).